

RESEARCH ARTICLE

Aerodynamic Effects of High-Speed Train Positions During Tunnel Exit Under Crosswind Conditions Using Computational Fluid Dynamics

S. Rajendran¹, I. A. Ishak^{1*}, M. Arafat¹, A. F. Mohammad², Z. M. Salleh¹, N. A. Samiran¹, M. N. M. Ja'at¹, S. Sulaiman¹

¹Faculty of Engineering Technology, University of Tun Hussein Onn Malaysia, Education Hub, Pagoh, 84600, Johor, Malaysia

²Department of Mechanical Precision Engineering, Malaysia-Japan International Institute of Technology (MJIT), Universiti Teknologi Malaysia (UTM), Jalan Sultan Yahya Petra, 54100, Kuala Lumpur, Malaysia

ABSTRACT - Strong crosswinds can cause catastrophic accidents like overturning and derailment in extreme circumstances, therefore the train's capacity to tolerate their impacts is crucial. Despite the significance of this issue, there exists a notable research gap in understanding the specific effects of various positions of a high-speed train within a tunnel on its aerodynamic loads and flow structure under different crosswind conditions. To address this gap, numerical simulations were performed using computational fluid dynamics. The crosswind angles (ψ) were 15° , 30° , 45° , and 60° and the number of coaches exiting the tunnel was one to three coaches, respectively. The incompressible flow around the train was simulated using the Unsteady Reynolds-Averaged Navier-Stokes (URANS) equations in conjunction with the k -epsilon (k - ϵ) turbulence model. The Reynolds number employed in the simulation was 1.3×10^6 , calculated based on the height of the train and the freestream velocity. With regard to aerodynamic performance due to the crosswind, force coefficients such as drag, side, and lift and moment coefficients of rolling, pitching, and yawing were measured. The higher crosswind angles including $\psi = 45^\circ$ and $\psi = 60^\circ$ cases produced the worse results of aerodynamic load coefficients compared to the lower crosswind angles of $\psi = 15^\circ$ and $\psi = 30^\circ$. For instance, the highest side force coefficient (C_s) was recorded at a crosswind angle of $\psi = 45^\circ$, with a value of 23.6. Meanwhile, the flow structure revealed that the leading coach of the train experienced intricate flow patterns during crosswinds, characterized by vortices and flow separation. These findings indicate that aerodynamic instabilities can potentially affect the overall performance of the train. Additionally, this increases the risk of derailment or overturning to be high, particularly when the majority of coaches are exiting the tunnel under strong crosswind conditions.

ARTICLE HISTORY

Received : 18th Mar. 2023

Revised : 17th Jan. 2024

Accepted : 09th Mar. 2024

Published : 20th June 2024

KEYWORDS

Aerodynamic characteristics

Computational fluid dynamics

Crosswind angle

High-speed train

Tunnel

1.0 INTRODUCTION

High-speed train (HST) is a kind of train transportation that goes substantially faster than conventional rail traffic due to an integrated system of specialized trains and dedicated railway tracks [1, 2]. Due to its speed and substantial transportation capacity, the HST network has experienced significant growth in recent decades. All these advantages, come at a cost. The aerodynamic performance of the train is strongly impacted by its speed, creating issues with operational performance and safety, especially when traveling near a tunnel [3–8]. Moreover, moving in the opposite direction of the wind provides a crosswind component on the item, increasing the apparent wind loads on the object [9–11]. A vehicle acts as if it is solely experiencing a lateral effect from the amount of the crosswind component [12]. When a train travels through a tunnel, the compressed air in the tunnel follows the train. Behind the train, a region of low pressure develops, bringing in outside air [13]. The impact of strong crosswinds on trains is a critical factor in ensuring the safety and stability of railway operations. Crosswinds can exert significant lateral forces on trains, potentially leading to catastrophic accidents such as derailments or overturning, particularly in extreme circumstances. Therefore, understanding the train's capacity to tolerate the impacts of strong crosswinds when exiting a tunnel is of utmost importance in ensuring the safety and reliability of railway transportation systems [14–19]. Real-life experiments require considerable expense and time to implement and also necessitate the researcher's time sacrifice in order to obtain the desired outcome [20, 21]. Using numerical analysis and data structures, computational fluid dynamics (CFD), a subfield of fluid mechanics, analyses and resolves issues involving fluid flows [3].

Previously, Miao *et al.* [1] employed improved delayed detached-eddy simulations (IDDES) to numerically investigate the aerodynamic performance of a high-speed train moving through tunnel junctions under strong crosswind conditions. Their study revealed notable variations in pressure distribution along the train body, with heightened pressures observed on the leeward side during tunnel entry and on the windward side during tunnel exit. Furthermore, at the junction locations, a slightly larger change in the pressure coefficient was noted, while the midsection of the tunnel experienced the most significant peak-to-peak pressure differentials. The integrated interaction between the moving train, tunnel, and crosswind led to alterations in the flow field both inside and outside the tunnel. Notably, due to the shielding effect of the tunnel walls, the crosswind's impact was limited to the exterior of the train, exerting a distinctive lateral force on this region[1].

*CORRESPONDING AUTHOR | I. A. Ishak | izuan@uthm.edu.my

Additionally, Yang et al. studied the sudden variation effect of aerodynamic loads and safety analysis of running trains when entering tunnels under crosswind, focusing on the transient characteristics and main factors of aerodynamic loads [22]. Li et al. confirmed through numerical simulation and field tests that the lateral vibration and aerodynamic drag of trains increased, and micro-pressure waves were produced at the tunnel exit when high-speed trains passed through tunnels [23]. These studies collectively underscore the significant impact of tunnel aerodynamics and crosswind conditions on high-speed trains. In addition, the study by Han et al. highlights the significance of the angle of attack of the oncoming flow in influencing the aerodynamics of high-speed trains [24]. The experimental results indicate that the aerodynamic characteristics of high-speed trains experience significant changes depending on the angle of attack, which is crucial when considering the effects of different crosswind angles on trains exiting the tunnels. Therefore, this study particularly focuses on the aerodynamic performance of HST at different train exiting positions and crosswind angles.

Now, to comprehensively investigate the effect of various positions of high-speed trains while exiting the tunnel on their aerodynamic loads and flow structure under different crosswind conditions, numerical simulations are performed using computational fluid dynamics. The crosswind angles (ψ) were 15° , 30° , 45° , and 60° and the number of coaches exiting the tunnel was one to three coaches, respectively.

2.0 METHODOLOGY

Figure 1 shows the flowchart of the CFD analysis of the current study. The tunnel utilized in this study was designed using SolidWorks software. Additionally, the Next-generation high-speed train, originally developed by the German Aerospace Center (DLR), served as the train model used for this investigation. Detailed dimensions of the train model and tunnel geometry are illustrated in Figure 2. The validation process commenced with a grid independence test and comparison with the previous study. The validation was conducted following the work [25] where only one and a half of the train model was used. However, for the case simulation, a completed train model was used.

The completion of the validation process leads to the real case simulation using the tunnel and different crosswind conditions as shown in Figure 3. The cases were categorized as Case A, B, and C, depending on the train's position upon exiting the tunnel. In Case A, one coach exited the tunnel, while Cases B and C involved the exit of two and three coaches, respectively. For each case, a total of 4 crosswind yaw angles were tested which were 15° , 30° , 45° , and 60° . An analysis was performed based on the results obtained from the simulation. The analysis was focused on the aerodynamic loads and flow structure around the train when it was exiting the tunnel under various crosswind conditions.

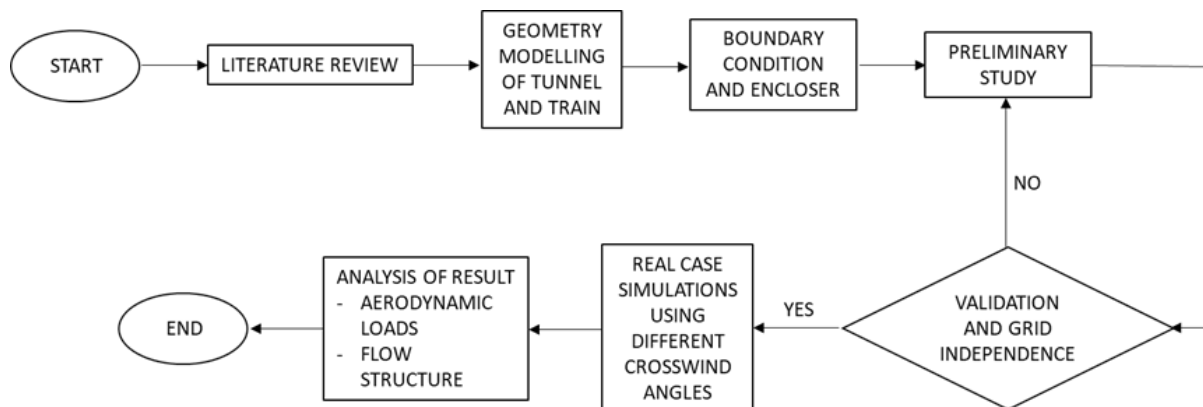


Figure 1. Flowchart of CFD analysis

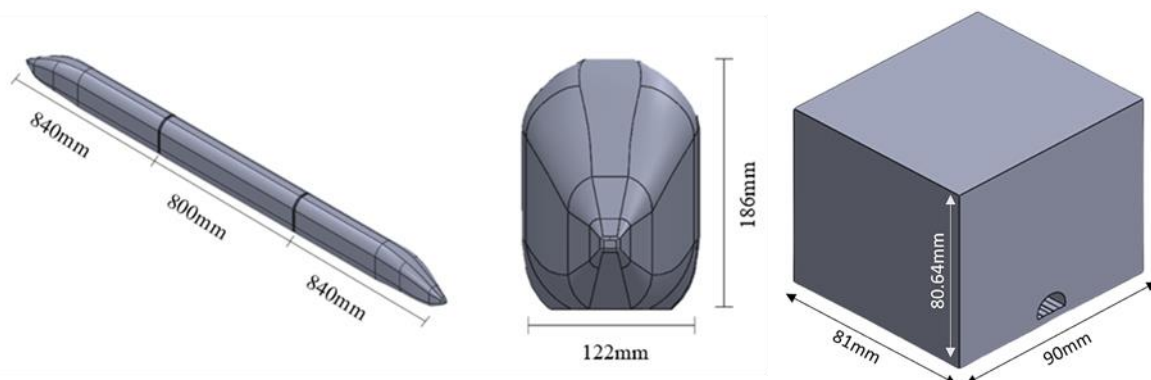


Figure 2. NG-HST and train model

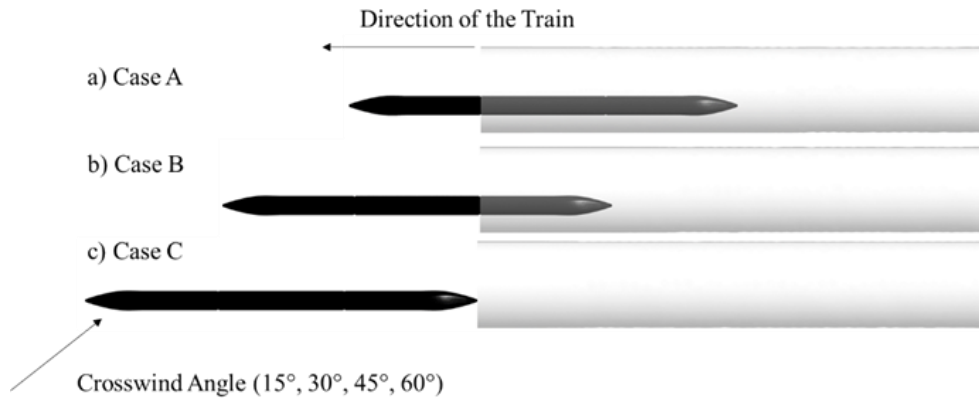


Figure 3. Cases involved in CFD simulation

2.1 Enclosure and boundary condition

The fluid domain or enclosure is used by analytical tools to mimic fluid. Figure 4 shows the computational domain for conducting the simulation. The location of the train model inside the enclosure is shown in Case B. The dimension of the enclosure and tunnel was followed by Miao *et al.* [1]. The computational domain was large enough to capture the flow field around the train.

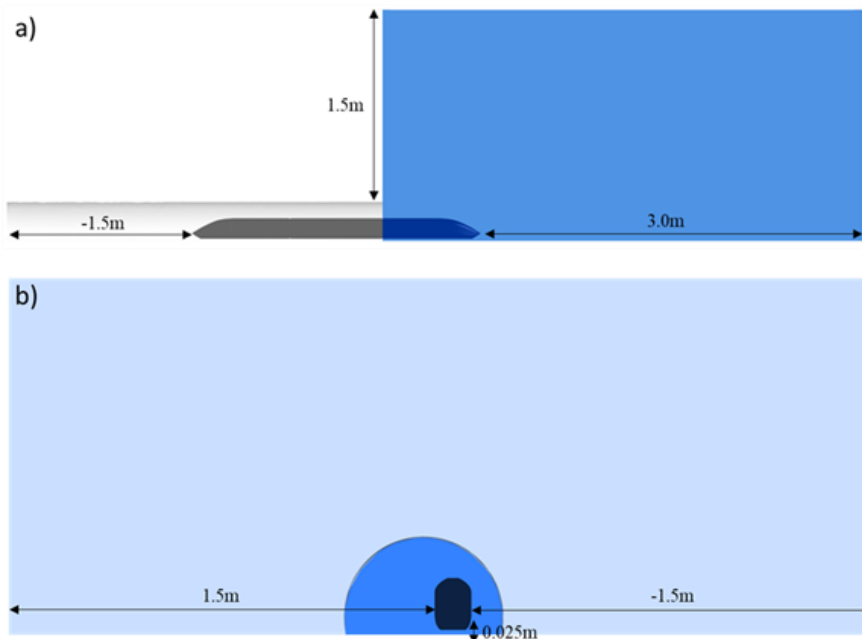


Figure 4. Train model in enclosure: a) front view; b) side view

The boundary conditions for the model, including velocity inlet, pressure outlet, vehicle surface, and symmetry sides, are defined upon the creation of the enclosure, as illustrated in Figure 5. A boolean feature in Ansys DesignModeler was employed to subtract the train solid from the fluid domain, retaining only the train surface. This approach was chosen as the current study specifically focuses on the external flow of the fluid. The Reynolds number employed in this investigation is $Re = 1.3 \times 10^6$ based on the characteristics' lengths which are the train height and fluid velocity. Details of boundary conditions are provided in Table 1.

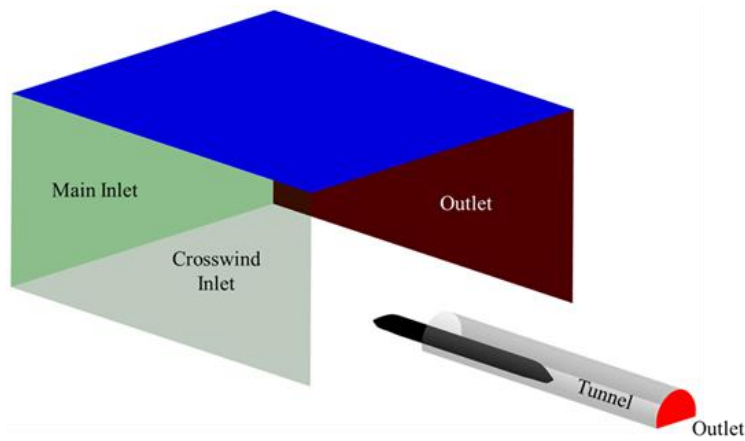


Figure 5. Boundary conditions used in numerical simulation

Table 1. Boundary condition parameters

Details	Boundary Condition	Value
Inlet	Velocity Inlet	111.11 m/s
Outlet	Pressure Outlet	0 Pa (gauge)
Symmetry	Wall Boundary	Stationary
Train Body	Wall Boundary	No slip
Reference Temperature		298K

2.2 Numerical method and solver setting

When a train is traveling at high speeds, the flow around it can be modeled as a three-dimensional incompressible flow process. The numerical simulation requires the use of an accurate turbulent transport equation. The Reynolds-averaged Navier-Stokes (RANS) simulation has been widely used as a numerical method for turbulent flow calculations due to its relatively high accuracy in predicting mean flow features and its more limited computational demands [26]. Therefore, in this study, Unsteady RANS based on the standard $k-\varepsilon$ turbulence model was used due to its effectiveness in capturing the turbulent behavior of the vehicles [27, 28]. The transient mode was chosen to explore the unsteady flow, utilizing an initial timestep of 0.004 as determined in a previous study [29]. Meanwhile, the maximum timestep was set to $1e-6$ to ensure that the Courant number was less than one. The y^+ value was within the 30-300 range, indicating that the mesh was sophisticated enough to capture near-wall flow mechanics. Furthermore, 20 iterations were computed for each time step. The simulation spanned four seconds, and the aerodynamic results were presented exclusively for the last timestep, simplifying the analysis process. The Coupled algorithm of pressure-velocity coupling was used, and the second-order scheme was chosen for the discretization of all variables.

2.3 Grid independence study

A grid independence study is a process in CFD where the sensitivity of the results to the size and structure of the computational grid is investigated. In order to determine the optimal grid resolution that provides accurate and reliable results with minimum computational cost, the CFD results were validated by contrasting the coefficient of drag (C_d) produced from the simulation with the outcomes of numerical analysis from three distinct meshes. Mesh parameters were changed to create coarse, medium, and fine mesh types as shown in Table 2. Details of the meshes on the train surface and computational domain can be seen in Figure 6. A Cartesian grid was adopted as the meshing approach. The use of a Cartesian grid as a meshing approach has been widely adopted in various CFD simulations. This approach offers several advantages, such as ease of implementation and reduced numerical diffusion of the mesh, making it promising for various engineering applications [30, 31]. C_d values obtained from different mesh resolutions and wind tunnel data from previous studies [25] are compared as shown in Table 3. The value of C_d started to converge after the medium mesh, where both medium and fine mesh had a C_d value of 0.178 nearly the same as the experimental value of 0.18. Thus, the medium mesh is used for the validation process.

Table 2. Parameters used for grid independence test

Type/ Parameter (mm)	Coarse	Medium	Fine
Mesh (max Size)	256	128	64
Face size (train surface)	20	10	5
Affected Diameter	2	4	8
Element Number	235,482	292,493	631,925

Table 3. Comparison results of different meshing resolutions and previous experiments

Parameter	Coarse	Medium	Fine	Experimental value [25]
Coefficient of drag (C_d)	0.19	0.178	0.178	0.18

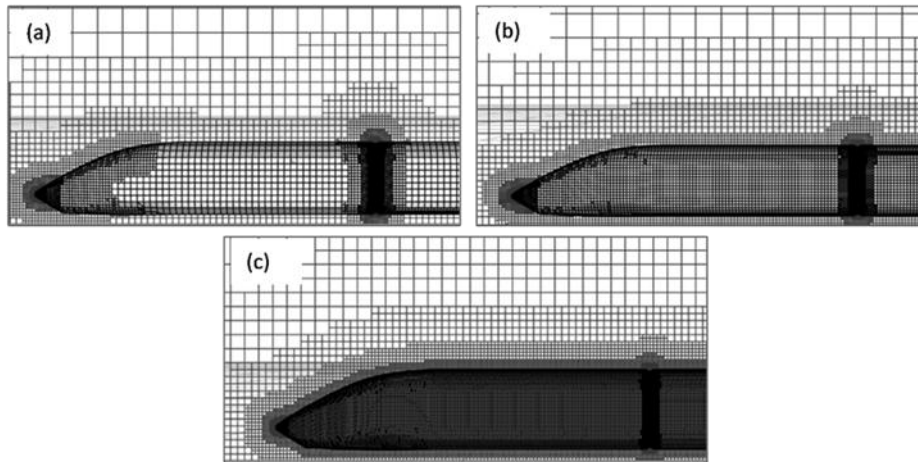


Figure 6. Result of different mesh qualities: a) coarse; b) medium; c) fine

3.0 RESULTS AND DISCUSSION

The results were analyzed in two main categories where the qualitative results included streamline and vortex formations due to the changes in pressure acting on the train body and the quantitative results included the coefficient of aerodynamic forces like drag, side, and lift as well as moments like pitch, yaw, and roll on the train body.

3.1 Qualitative Results

Figure 7 and Figure 8 show the top view of streamlines superimposed on the pressure contour for crosswind angles (ψ) of 15° , 30° , 45° , and 60° . As the crosswind approaches the side of the train body, the flow is disrupted and forced to split towards the top and bottom of the train. This flow separation causes higher and lower pressure regions due to the difference in velocity of the crosswind. Pressure is inversely proportional to velocity [32]. When the crosswind flows from the windward side, it is disrupted when it reaches the side of the train body, thus it greatly reduces the crosswind velocity. This phenomenon is a result of the aerodynamic interaction between the crosswind and the train body. The disruption of the crosswind as it reaches the train body is a complex process that involves the generation of vortices and changes in pressure distribution. The sudden drop in velocity causes the formation of a higher-pressure region at the windward side [33]. When a train is subjected to a crosswind, the airflow around the train is disturbed, leading to various aerodynamic effects. The disruption of the crosswind flow upon hitting the side wall of the train is a critical aspect of train aerodynamics.

The largest amount of low-pressure region at the leeward side of the train can be seen in the case of a $\psi = 60^\circ$ crosswind angle when all three coaches (Case C) of the train exit the tunnel. The increase in crosswind velocity at the leeward side of the coach is a result of the larger vortices formed at the higher crosswind angle. These vortices entrain more air from the surrounding flow, leading to an increase in the crosswind velocity at the leeward side of the coach. This increase in crosswind velocity further contributes to the reduction in pressure at the leeward side of the coach. In contrast, for Case C, where all the coaches of the train exit the tunnel under a $\psi = 15^\circ$ crosswind angle, the lower pressure region at the leeward side of the train is much lesser compared to the one at a $\psi = 60^\circ$ crosswind angle. This shows that higher crosswind angles have more effects on the vortex formation at the leeward side of the train compared to the number of coaches exposed to the crosswind. Furthermore, Zhang et al. (2017) highlighted the impact of crosswinds on the vortex structure, emphasizing that the vortex formation is dependent on the yaw angle [34].

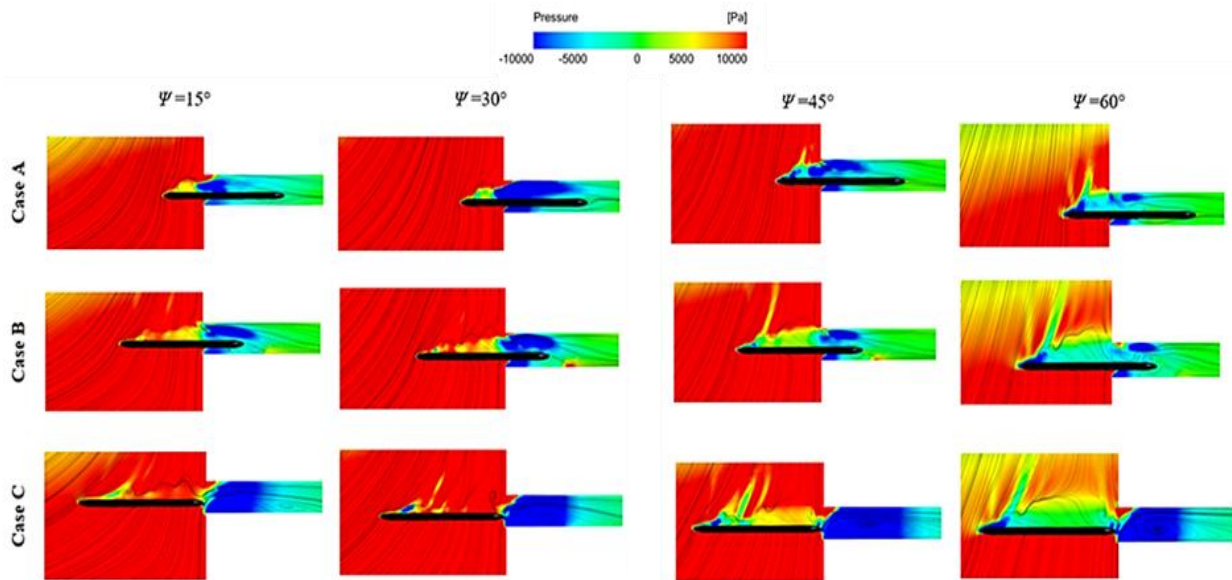


Figure 7. Streamlines superimposed on the pressure contour for different crosswind angles

Based on the vortex formation for different crosswind angles as shown in Figure 8, the intensity of vortex formation is the highest at the frontal area of the train body and increases along with the crosswind angle while being lowest at the last coach of the train. This shows that when compared to regions, the frontal part of the train is most affected by the aerodynamic loads due to crosswind. The formation of vortices at the frontal area of a train body and its increase along with the crosswind angle, while being lowest at the last coach of the train, is a complex phenomenon influenced by various factors. Guo et al. demonstrated that the vortex formation length increases significantly with the twisted angle of a cylinder, indicating a relationship between the geometry of the body and the intensity of vortex formation [35]. Other than that, it is also suggested that the vortex formation inside the tunnel is at the lowest intensity when all three coaches (Case C) of the train exit the tunnel. When the whole train body exits the tunnel, there is less flow separation, causing a smaller vortex to be formed between the rear end of the train and the tunnel end. In addition, it can be concluded that the vortex intensity is indeed affected by the number of coaches, with a higher number of coaches leading to a more intense vortex formation.

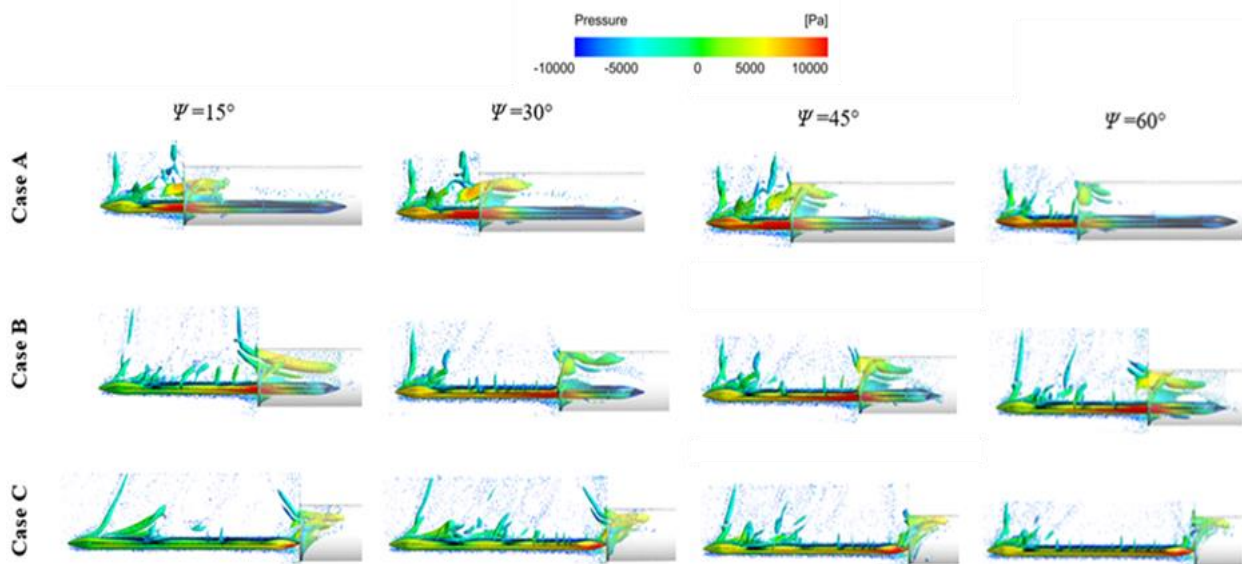


Figure 8. Vortex core for different crosswind angles (top-view)

Figures 9 and 10 display pressure contours alongside velocity streamlines at various locations (front-view). To analyze the pressure characteristics, a plane (P) was sliced through the middle of each coach, yielding Case A for one coach (P1), Case B (P2, P3), and Case C (P4, P5, P6). This flow separation causes higher and lower pressure regions due to the difference in the velocity of the crosswind. When the crosswind flows from the windward side, it is disrupted when it reaches the side of the train body, thus it greatly reduces the crosswind velocity. The sudden drop in velocity causes the formation of a higher-pressure region at the windward side.

The disruption of crosswind flow upon hitting the side wall of the train causes the airflow to split, with one component directed towards the top and another towards the bottom of the train. Before reaching the leeward side, a region of lower pressure forms at the top of the train body due to flow separation. This occurs because the crosswind, having its velocity reduced upon interaction with the train side wall, gains space to move freely toward the top of the train body, resulting in increased velocity. Simultaneously, another component of the flow is directed towards the bottom surface, creating a separation of flow underneath the train model and consequently generating a low-pressure region.

Moreover, direct impact which causes flow separation leads to the formation of reverse flow. This reverse flow field has high velocity and thus produces a low-pressure region surrounding the vortex formation area. The size of the vortex increases along with the increase in the angle of crosswind and also the number of coaches exiting the tunnel. For instance, the largest vortex can be seen in Case C, P4 as shown in Figure 10, where the angle of crosswind is $\psi = 60^\circ$ and all three train coaches exit the tunnel while, the smallest vortex is formed when only one coach is exiting with the crosswind angle of $\psi = 15^\circ$ as shown in Case A, P1 (Figure 9).

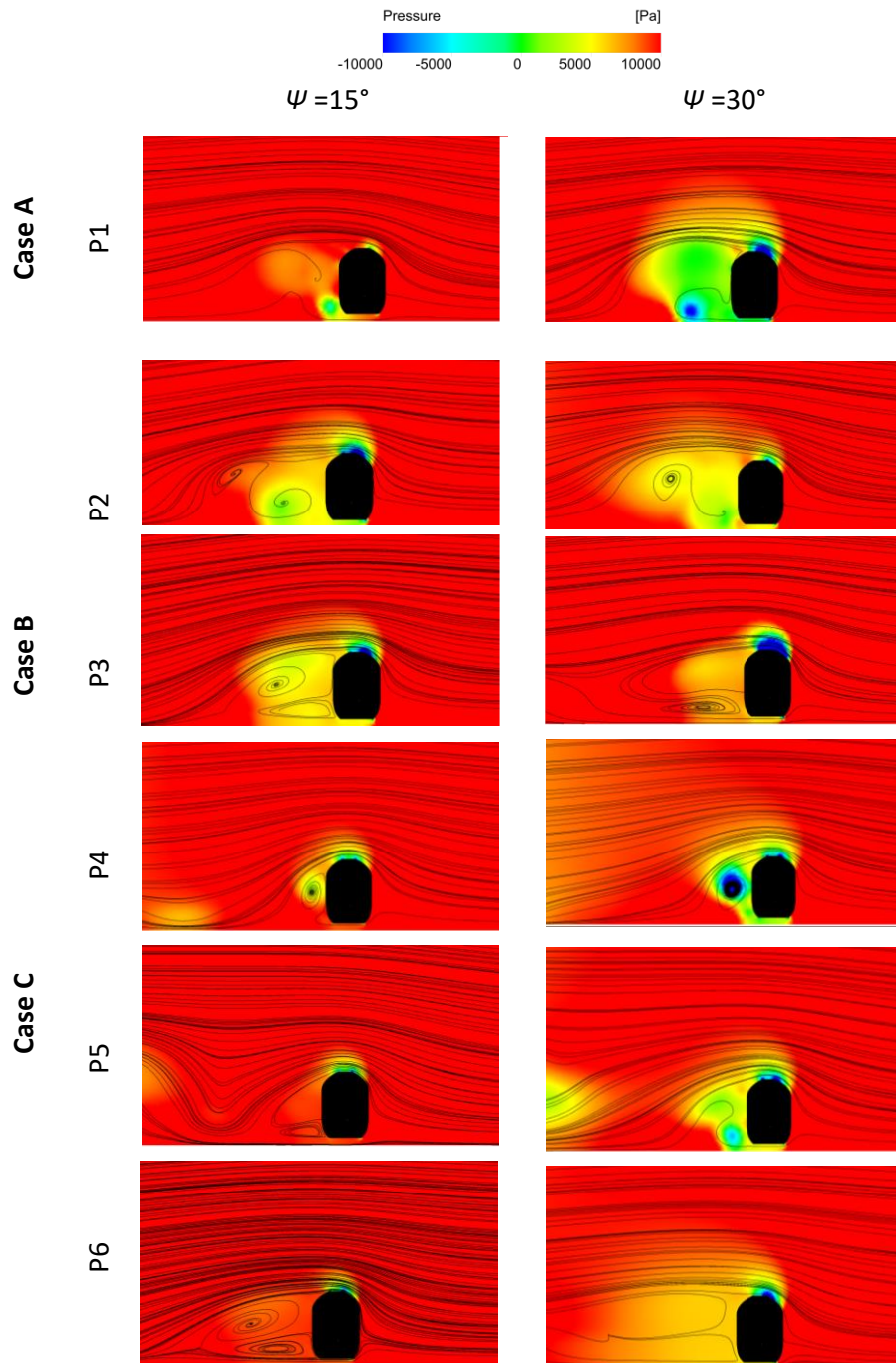


Figure 9. Streamlines superimposed on the pressure contour for low crosswind angle (front-view) sliced at the middle of each coach. Case A (P1), Case B (P2, P3), and Case C (P4, P5, P6)

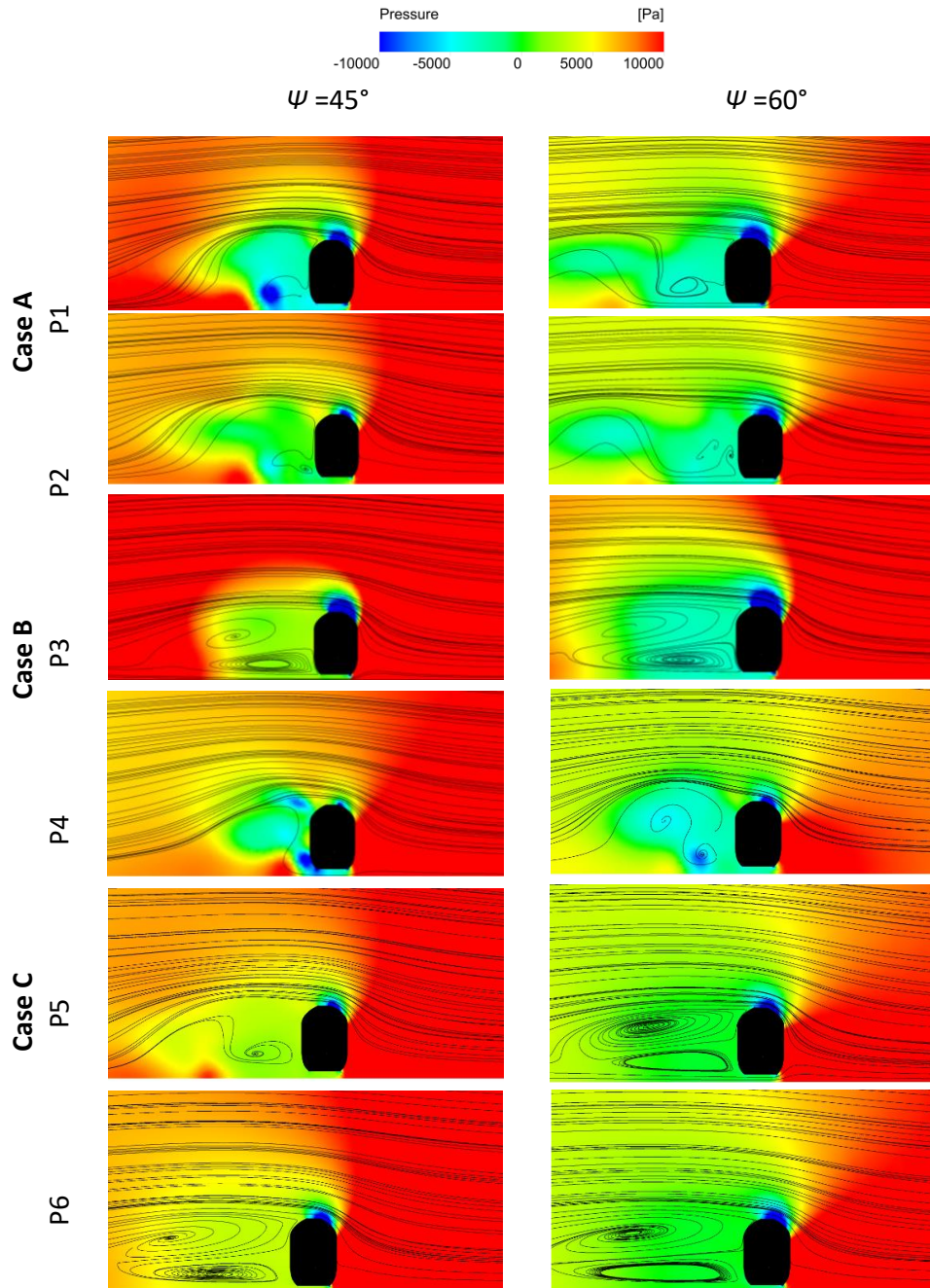


Figure 10. Streamlines superimposed on the pressure contour for high crosswind angle (front view) sliced at the middle of each coach. Case A (P1), Case B (P2, P3), and Case C (P4, P5, P6)

3.2 Quantitative Result

Figure 11 shows the changes in drag coefficient (C_d), lift coefficient (C_l), and side force coefficient (C_s) when the yaw angles of crosswind change along with the number of train coaches exiting the tunnel. The graph shows that the drag force coefficient is directly proportional to the number of train coaches exiting the tunnel. The value of C_d was lowest when 1 coach exited and highest when 3 coaches exited the tunnel. Meanwhile, when the number of coaches is kept constant, the C_l increases gradually from $\psi = 15^\circ$ to $\psi = 45^\circ$ and then decreases or has minimal changes when encountered with a $\psi = 60^\circ$ crosswind angle. This trend also follows when the crosswind yaw angle is kept constant while the number of train coaches exiting the tunnel increases. In contrast, the C_s increases gradually from $\psi = 15^\circ$ to $\psi = 45^\circ$ while having very minimal changes between $\psi = 30^\circ$ and $\psi = 45^\circ$, then decreases when encountered with a $\psi = 60^\circ$ crosswind angle. For instance, during the crosswind angle of $\psi = 45^\circ$, the C_s increased from 14.3241 to 19.9515 and then to 23.5912 when 3 coaches exited the tunnel. This shows that a crosswind yaw angle of $\psi = 45^\circ$ has the highest value of C_s as the number of coaches increases. Similar results were also observed by other researchers. For instance, the research by Niu et al. investigated the aerodynamic behavior of high-speed trains under crosswind conditions. The study highlighted the significance of crosswind yaw angle on the lateral forces experienced by the train. At a yaw angle of 45° , the train's exposure to the crosswind is maximized, potentially leading to increased lateral forces [36].

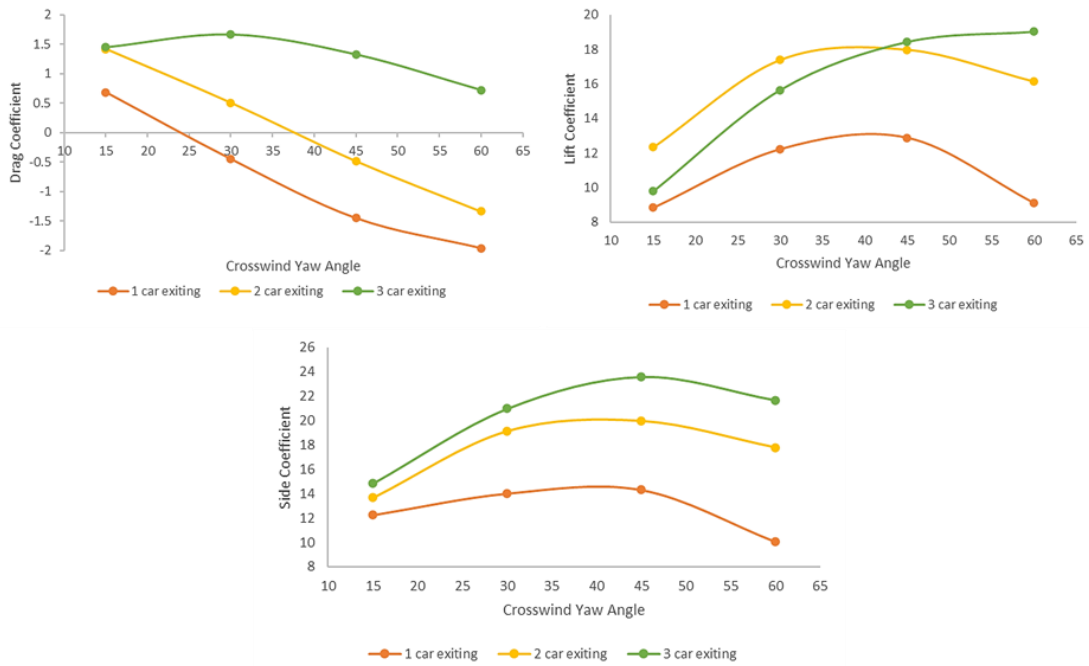


Figure 11. Comparison of drag coefficient (C_d), lift coefficient (C_l), and side force coefficient (C_s) for different numbers of NG-HST coaches exiting the tunnel under crosswind conditions

Figure 12 shows the changes in yaw moment coefficient (C_{YA}), rolling moment coefficients (C_{RL}), and pitching moment coefficient (C_{PI}) when the angles of crosswind change along with the number of train coaches exiting the tunnel. When the number of coaches remained the same, a decreasing trend was recorded between crosswind angles of $\psi = 15^\circ$ to $\psi = 45^\circ$ before increasing when encountered with $\psi = 60^\circ$ crosswind. It is noticeable that the C_{YA} increases at $\psi = 60^\circ$ crosswind is the steepest when two coaches exit the tunnel. Meanwhile, when compared to other moment forces, C_{RL} recorded the most minimal changes when encountered with different crosswinds. The C_{RL} decreases along with the increase in the number of coaches exiting the tunnel and crosswind angles. Moreover, the highest C_{RL} of -0.2435 was recorded when one coach was exiting the tunnel with $\psi = 15^\circ$ of crosswind while the lowest was when three coaches exited the tunnel under $\psi = 60^\circ$ crosswind condition with a value of -0.5564. In contrast, when comparing the overall effect of pitching, it is the highest when one coach is exiting the tunnel while lowest when three coaches exit the tunnel under various crosswind conditions. With respect to the current study's results, Asress & Svorcan demonstrated that increasing the yaw angle results in the creation of a low-pressure region on the leeward side of the train, causing high side force and roll moment [37]. The roll moment coefficient value decreases with an increasing crosswind angle, as observed in the current study. This phenomenon is attributed to the effects of the tunnel exiting conditions.

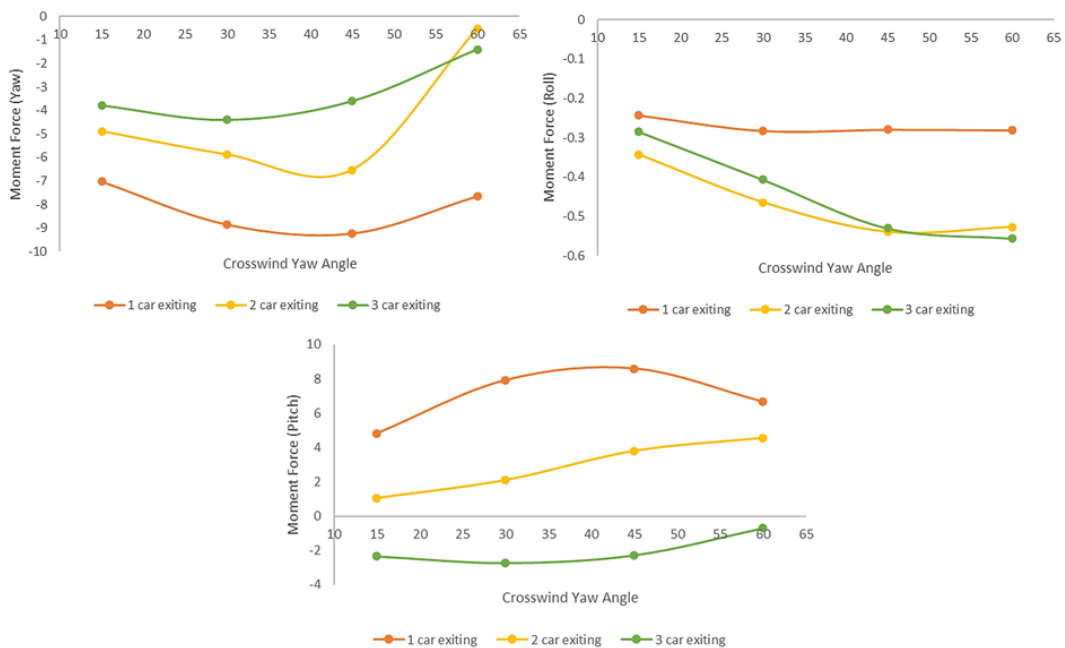


Figure 12. Comparison of yaw moment coefficient (C_{YA}), rolling moment coefficient (C_{RL}), and pitching moment coefficient (C_{PI}) for different numbers of NG-HST coaches exiting the tunnel under crosswind conditions

4.0 CONCLUSION

In this study, investigations on the effect of various positions of high-speed trains (HST) while exiting the tunnel on aerodynamic loads and flow structures under different crosswind conditions were conducted using computational fluid dynamics (CFD) analysis. The scope of this study was limited to four crosswind conditions to represent the effect of lower crosswind conditions ($\psi = 15^\circ$ and $\psi = 30^\circ$) and higher crosswind conditions ($\psi = 45^\circ$ and $\psi = 60^\circ$).

The higher crosswind angles including $\psi = 45^\circ$ and $\psi = 60^\circ$ cases produced worse results of aerodynamic load coefficients compared to the lower crosswind angles of $\psi = 15^\circ$ and $\psi = 30^\circ$. Meanwhile, the side force coefficient exhibited an upward trend across all cases as crosswind angles increased, reaching its peak at $\psi = 45^\circ$. This suggests that $\psi = 45^\circ$ is the most critical crosswind angle for the train when exiting a tunnel. In contrast, the simulation results showed that roll and pitch moments were the highest in cases where only one coach exited the tunnel, increasing along with the crosswind angle. In terms of the flow structure, the results revealed that the leading coach of the train experienced complex flow patterns during crosswinds, characterized by vortices and flow separation. These findings indicate aerodynamic instabilities that can potentially affect the overall performance of the train.

These findings hold significant implications for enhancing safety measures in the technical aspects of general train operation. As an outcome, aerodynamic loads are majorly influenced by crosswind yaw angles. In this study, we focused on the aerodynamic performance of a train when exiting a tunnel. However, it is important to include the effects of crosswind while the train is entering and passing through the tunnel to get a complete analysis of different crosswind conditions.

5.0 ACKNOWLEDGEMENT

This research was supported by the Ministry of Higher Education (MOHE) through Fundamental Research Grant Scheme (FRGS) (FRGS/1/2022/TK02/UTHM/03/1).

6.0 REFERENCES

- [1] X. Miao, K. He, G. Minelli, J. Zhang, G. Gao, H. Wei, et al., "Aerodynamic performance of a high-speed train passing through three standard tunnel junctions under crosswinds," *Applied Sciences*, vol. 10, no. 11, p. 3664, 2020.
- [2] I.A. Ishak, N. Maruai, F.M. Sakri, R. Mahmudin, N.A. Samiran, S. Sulaiman, et al., "Numerical analysis on the crosswind influence around a generic train moving on different bridge configurations," *Journal of Advanced Research in Fluid Mechanics and Thermal Sciences*, vol. 89, no. 2, pp. 76–98, 2022.
- [3] M. Arafat and I.A. Ishak, "CFD analysis of the flow around simplified next-generation train subjected to crosswinds at Low Yaw Angles," *CFD Letters*, vol. 14, no. 3, pp. 129–139, 2022.
- [4] X. Huo, T. Liu, M. Yu, Z. Chen, Z. Guo, W. Li, et al., "Impact of the trailing edge shape of a downstream dummy vehicle on train aerodynamics subjected to crosswind," *Proceedings of the Institution of Mechanical Engineers, Part F: Journal of Rail and Rapid Transit*, vol. 235, no. 2, pp. 201–214, 2021.
- [5] A. Hajipour, A.M. Lavasani, and M.E. Yazdi, "Investigation of wall function effects on aerodynamic characteristics of turbulent flow around a simplified high-speed train," *International Journal of Heat and Technology*, vol. 39, no. 1, pp. 309–318, 2021.
- [6] I.A. Ishak, M.S.M. Ali, and S.A.Z.S. Salim, "Numerical simulation of flow around a simplified high-speed train model using OpenFOAM," *IOP Conference Series: Materials Science and Engineering*, vol. 152, no. 1, p. 012047, 2016.
- [7] M. Arafat, I.A. Ishak, A.F. Mohammad, A. Khalid, M.N.M. Jaát, and M.F. Yasak, "Effect of Reynolds number on the wake of a next-generation high-speed train using CFD analysis," *CFD Letters*, vol. 15, no. 1, pp. 76–87.
- [8] C. Baker, "The flow around high-speed trains," *Journal of Wind Engineering and Industrial Aerodynamics*, vol. 98, no. 6–7, pp. 277–298, 2010.
- [9] M.M. Fagner, K.A. Weinman, R. Deiterding, U. Fey, and C. Wagner, "Numerical and experimental studies of train geometries subject to cross winds," *Civil-Comp Proceedings 2014* [Online] 2014.
- [10] M.N. Kamal, I.A. Ishak, N. Darlis, N.A. Samiran, R. Mahmudin, R.A. Rashid et al., "Effect of crosswinds on aerodynamic characteristics of a generic train model using ANSYS," *Journal of Industry, Engineering and Innovation*, vol. 2, no. 1, pp. 1–12, 2020.
- [11] A.N. Nazri, I.A. Ishak, N. Darlis, Z.M. Salleh, S.F. Zainal, S. Sulaiman et al., "Aerodynamic analysis on the effects of different type of train's nose design using ANSYS Software," *Journal of Industry, Engineering and Innovation*, vol. 1, no. 1, pp. 1–10, 2019.
- [12] M.M. Fagner and R. Deiterding, "Investigating cross-wind stability of high-speed trains with large-scale parallel CFD," *International Journal of Computational Fluid Dynamics*, vol. 30, no. 6, pp. 402–407, 2016.

- [13] I.A. Ishak, M.S.M. Ali, M.F.M. Yakub, and S.A.Z.S. Salim, "Effect of crosswinds on aerodynamic characteristics around a generic train model," *International Journal of Rail Transportation*, vol. 7, no. 1, pp. 1–32, 2018.
- [14] M.N.F. Kamal, I.A. Ishak, N. Darlis, D.S.B. Maji, S.L. Sukiman, R.A. Rashid, et al., "A review of aerodynamics influence on various car model geometry through CFD techniques," *Journal of Advanced Research in Fluid Mechanics and Thermal Sciences*, vol. 88, no. 1, pp. 109–125, 2021.
- [15] C. Baker, H. Hemida, S. Iwnicki, G. Xie, and D. Ongaro, "Integration of crosswind forces into train dynamic modelling," *Proceedings of the Institution of Mechanical Engineers, Part F: Journal of Rail and Rapid Transit*, vol. 225, no. 2, pp. 154–164, 2011.
- [16] I.A. Ishak, M.S.M. Ali, F.M. Sakri, F.H. Zulkifli, N. Darlis, R. Mahmudin, et al., "Aerodynamic characteristics around a generic train moving on different embankments under the influence of crosswind," *Journal of Advanced Research in Fluid Mechanics and Thermal Sciences*, vol. 61, no. 1, pp. 106–128, 2019.
- [17] I.A. Ishak, M.S.M. Ali, and S.A.Z.S. Salim, "Numerical simulation of flow around a simplified high-speed train model using OpenFOAM," *IOP Conference Series: Materials Science and Engineering*, vol. 152, no. 1, p. 012047, 2016.
- [18] I.A. Ishak, R. Mahmudin, N. Samiran, Z. Salleh, and N. Darlis, "Safety guideline for a generic train travelling on different platform scenarios under the influence of crosswind," *International Journal of Advanced Trends in Computer Science and Engineering*, vol. 9, no. 1.4, pp. 138–150, 2020.
- [19] J. Herb, U. Hoppmann, C. Heine, and T. Tielkes, "A new approach to estimate the wind speed probability distribution along a railway track based on international standards," *Journal of Wind Engineering and Industrial Aerodynamics*, vol. 95, no. 9–11, pp. 1097–1113, 2007.
- [20] J. Du, Q. Fang, J. Wang, and G. Wang, "Influences of high-speed train speed on tunnel aerodynamic pressures," *Applied Sciences*, vol. 12, no. 1, p. 303, 2021.
- [21] H. Li, M. Yu, Q. Zhang and H. Wen, "A numerical study of the aerodynamic characteristics of a high-speed train under the effect of crosswind and rain," *Fluid Dynamics and Materials Processing*, vol. 16, no. 1, pp. 77–90, 2020.
- [22] W. Yang, E. Deng, Z. Zhu, M. Lei, C. Shi and H. He, "Sudden variation effect of aerodynamic loads and safety analysis of running trains when entering tunnel under crosswind," *Applied Sciences*, vol. 10, no. 4, p. 1445, 2020.
- [23] W. Li, H. Wang, Z. Wen, X. Du, L. Wu, X. Li et al., "An investigation into the mechanism of metro rail corrugation using experimental and theoretical methods," *Proceedings of the Institution of Mechanical Engineers, Part F: Journal of Rail and Rapid Transit*, vol. 230, no. 4, pp. 1025–1039, 2016.
- [24] Y. Han, Y. Liu, P. Hu, C.S. Cai, G. Xu et al., "Effect of unsteady aerodynamic loads on driving safety and comfort of trains running on bridges," *Advances in Structural Engineering*, vol. 23, no. 13, pp. 2898–2910, 2020.
- [25] M.M. Fragner, K.A. Weinman, R. Deiterding, U. Fey and C. Wagner, "Comparison of industrial and scientific CFD approaches for predicting cross wind stability of the NGT2 model train geometry," *International Journal of Railway Technology*, vol. 4, no. 1, pp. 1–28, 2015.
- [26] P. Marsh, D. Ranmuthugala, I. Penesis, and G. Thomas, "Three-dimensional numerical simulations of straight-bladed vertical axis tidal turbines investigating power output, torque ripple and mounting forces," *Renewable Energy*, vol. 83, pp. 67–77, 2015.
- [27] B. Diedrichs, M. Sima, A. Orellano, and H. Tengstrand, "Crosswind stability of a high-speed train on a high embankment," *Proceedings of the Institution of Mechanical Engineers, Part F: Journal of Rail and Rapid Transit*, vol. 221, no. 2, pp. 205–225, 2007.
- [28] F. Cheli, F. Ripamonti, D. Rocchi, and G. Tomasini, "Aerodynamic behaviour investigation of the new EMUV250 train to cross wind," *Journal of Wind Engineering and Industrial Aerodynamics*, vol. 98, no. 4–5, pp. 189–201, 2010.
- [29] M. Arafat and I.A. Ishak, "Aerodynamic performance of a next-generation high-speed train under transient crosswind," OSF Preprint 2023[Online] 2023 [cited 2023]. Available at: www.osf.io/u3mqb.
- [30] K. Nakahashi, and L. Kim, "High-density mesh flow computations by building-cube method," *Computational Fluid Dynamics 2004*, Springer, Berlin, Heidelberg, pp. 121–26, 2006.
- [31] M. Sosnowski, R. Gnatowska, K. Grabowska, J. Krzywański, and A. Jamrozik, "Numerical analysis of flow in building arrangement: Computational domain discretization," *Applied Sciences (Switzerland)*, vol. 9, no. 5, 2019.
- [32] M.N.F. Kamal, I.A. Ishak, N. Darlis, N.M. Maruai, R. Jamian, R.A. Rashid et al., "Flow structure characteristics of the simplified compact car exposed to crosswind effects using CFD," *Journal of Advanced Research in Applied Sciences and Engineering Technology*, vol. 28, no. 1, pp. 56–66, 2022.
- [33] K. Ye, and R.X. Li, "The analysis of aerodynamic characteristics of the high-speed train in different railway conditions under crosswinds," *Advanced Materials Research*, vol. 774–776, pp. 58–63, 2013.
- [34] J. Zhang, K. He, X. Xiong, J. Wang, and G. Gao, "Numerical simulation with a DES approach for a high-speed train subjected to the crosswind," *Journal of Applied Fluid Mechanics*, vol. 10, no. 5, pp. 1329–1342, 2017.

- [35] C. Guo, H. Guo, J. Hu, K. Song, W. Zhang, and W. Wang, "Large eddy simulation of flow over wavy cylinders with different twisted angles at a subcritical Reynolds number," *Journal of Marine Science and Engineering*, vol. 7, no. 7, p. 227, 2019.
- [36] J. Niu, D. Zhou, and X. Liang, "Numerical investigation of the aerodynamic characteristics of high-speed trains of different lengths under crosswind with or without windbreaks," *Engineering Applications of Computational Fluid Mechanics*, vol. 12, no. 1, pp. 195–215, 2018.
- [37] M.B. Asress, and J. Svorcan, "Numerical investigation on the aerodynamic characteristics of high-speed train under turbulent crosswind," *Journal of Modern Transportation*, vol. 22, no. 4, pp. 225–234, 2014.